UNIVERSITY OF
BATH

University of Bath

Closed loop control of force operation in a novel self-sensing dielectric elastomer actuator

R Zhang *, P Iravani, P Keogh

Department of Mechanical Engineering, University of Bath, Bath BA27AY, UK;
P.Iravani@bath.ac.uk; P.S.Keogh@bath.ac.uk
* Correspondence: R.Zhang2@bath.ac.uk; Tel: +44 1225 385958

Abstract. Closed loop feedback is essential in achieving the precise control of dielectric elastomer actuators (DEAs) due to their inherent nonlinear viscoelasticity. A novel self-sensing mechanism that uses capacitive sensing to detect the actuation of force in a dielectric elastomer sensing actuator (DESA) is proposed in this paper. In contrast to a conventional self-sensing DEA, it consists of an electro-active region (AR) for the actuation together with an independent electro-sensing region (SR). By doing so, the self-sensing mechanism does not exhibit long-term drift in the correlation between the structural deformation and the capacitive change, which is commonly found in conventional self-sensing DEAs. The results show that the proportional-integral (PI) controlled DESA performs effectively under uniaxial actuation. The DESA can suppress the relaxation of the viscoelastic DE and thus enable a constant force output. It also shows that the sensing capacity of the DESA can be enhanced further with appropriate electrode arrangement and motion-constraining. Furthermore, the results show that the DESA senses the off-plane expansion distinctly compared with the in-plane deformation, which helps to detect any wrinkling of the structure.

Keywords: DEA, self-sensing, sensors, electrode optimization, closed loop control

1. Introduction

As a next generation soft actuation technology, dielectric elastomer actuation is of particular interest because of its similar capability to human muscle [1-8]. It consists of a dielectric elastomer (DE) film that is sandwiched between compliant electrodes. When a high voltage is applied across the electrodes, the structure responds in planar expansion with contraction in thickness. The outstanding material properties in the electro-mechanical coupling make the DE ideal for displacement/strain sensing [9,10], energy harvesting [11-13], as well as actuation [14-17]. A dielectric elastomer actuator (DEA) has demonstrable muscle-like capability in bio-inspired robots [18-21], tuneable optics [22-26], flexible robotic legs [27], and lighter-than-air vehicles [28]. However, the advancement in other applications is hindered by the viscoelasticity of the DE. For a typical elastomer such as VHB 4910 from 3M, the time-dependent stress-strain relationship causes long-term relaxation upon loading and sluggish responses, which limit high-frequency actuation. The force and displacement control of the DEA require feedback to achieve the required performance.

Closed loop operation has been applied to adjust actuation force and strain [29-32]. These works show that with external sensors, motion control can be achieved with proportional-integral-derivative (PID) controllers. The DEA-based tuneable grating is a typical example [25]. A compliant grating is placed on the DEA so that it deforms with the DE as the voltage is applied. It uses the first-order diffraction angle of the grating that is measured by a photo-diode to drive the DEA to the desired deformation. However, the main drawbacks are the complexity and high cost of the system. Furthermore, it contradicts the intention in utilizing a low-cost polymeric actuation approach.

Another alternative is to use a DEA as a motion sensor, to form a self-sensing DEA. Past work has focused on use a single electro-active region (AR) to perform both the actuation and the sensing. Resistive sensing is commonly avoided as the conductivity of the electrode depends on many factors, including the electrode material, the electrode configuration and the deformation of the DE [33]. Capacitive sensing is better because the capacitance depends only on the geometry of the capacitor and the electrode coverage [34,35]. The capacitance is measured typically by using a high frequency AC signal that is superimposed on the actuation voltage [10,36-39]. Other approaches use pulse width modulation to measure the capacitive discharge rate [40], and step voltage application to measure charge [41]. However, these publications show also that large deformations of the DE and coupled high electric fields during the operation cause complex changes in the electrode resistance and dielectric resistance, which leads to the unexpected capacitive response in the actuation [42-45].

This paper presents the concept of a dielectric elastomer sensing actuator (DESA), a self-sensing DE actuator that utilizes separate electrode regions for sensing and actuating. By doing so, it demonstrates that the capacitive sensing mechanism in the DESA performs effectively and does not suffer from the previously mentioned deficiencies. Moreover, the performance of the structure with alternative electrode arrangements and motion constraining are also assessed. Finally, the challenges in implementing the DESA structure, the effects of electrode coverage and off-plane actuation on sensing resolution of the DESA are studied.
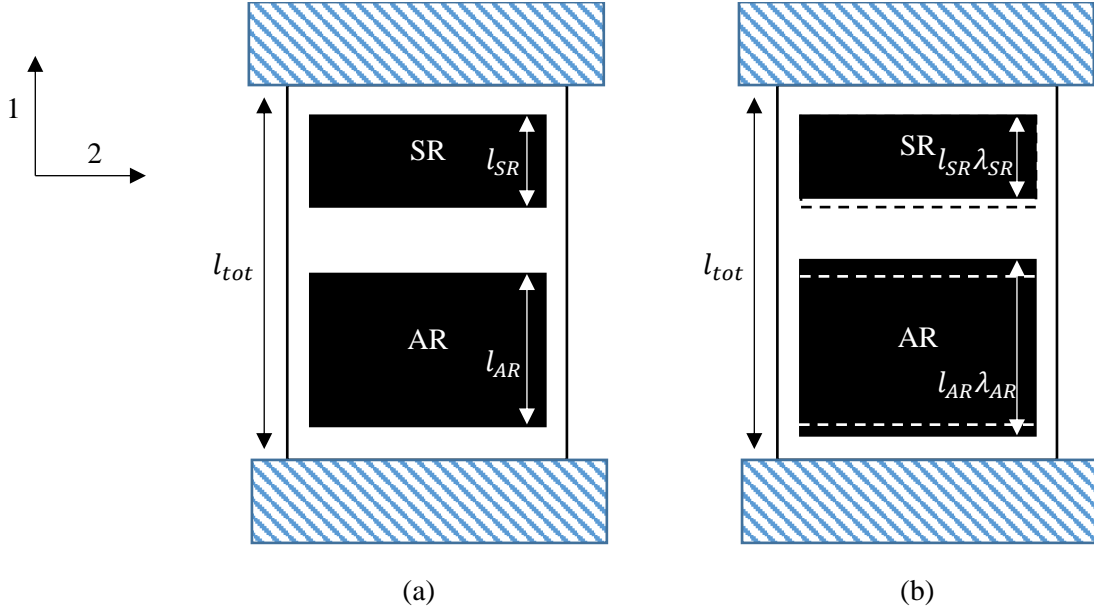
Figure 1. Geometric correlation of the DESA: (a) the undeformed state and (b) the actuated state.

2. Theory

2.1 Capacitive sensing in the DESA

In the structure of a DESA, the high voltage application across the AR deforms the entire elastomer. The electro-sensing region (SR) detects such deformation, and its capacitance changes correspondingly. For an understanding of the self-sensing mechanism, the correlation of $\lambda_{AR} = f(C)$ is derived, where C is the capacitance in the SR and λ_{AR} is the voltage induced mechanical deformation in the AR. Figure 1 shows the geometric correlation of the DESA with and without the voltage application. The DESA is pre-strained and constrained in direction 1, serving as a linear actuator. It is assumed that the SR only detects the deformation of the AR in direction 1 (e.g. the sensing is independent of the lateral expansion of the AR and the resulting inhomogeneous thickness due to the actuation). This assumption was validated from the experimental results (section 4.1, figure 5b) when a 15 mm gap was set between the electrode regions. Moreover, the overall length of the film in direction 1 is assumed to be constant as in the experiment the DESA was fixed on the top and clamped to a load cell on the bottom that was much stiffer than the DESA. When the voltage is applied, assuming the AR expands uniformly in the strain of λ_{AR} (Figure 1b), the corresponding strain in the SR, λ_{SR} is given by

$$\lambda_{SR} = \frac{l_{tot} - l_{AR}\lambda_{AR}}{l_{tot} - l_{AR}} \tag{1}$$

where l_{tot} is the total length of the film, l_{AR} is the length of the AR and λ_{AR} is the voltage-induced strain in l_{AR}. Taking the incompressibility of the elastomer, the volume associated with the SR implies that

$$\lambda_{SR}\lambda_h\lambda_w = 1 \tag{2}$$

where λ_w and λ_h are the resulting strains of the SR in direction 2 and the direction of thickness, respectively. Assuming that the elastomer is isochoric, the uniaxial loading condition gives

$$\lambda_w = \lambda_h = 1/\sqrt{\lambda_{SR}} \tag{3}$$

The capacitance of the SR in the undeformed state is therefore given by

$$C_0 = \frac{\varepsilon_0 \varepsilon_r w l_{SR}}{h} \tag{4}$$

where ε_0 is the permittivity of free space, ε_r is the relative permittivity of the elastomer and w, h are the width and the thickness of the SR, respectively. Substituting equation (3) into (4) gives the resultant capacitance in the actuated state C_a as

$$C_a = C_0 \lambda_{SR} \tag{5}$$

Substituting equation (1) into (5) gives the strain in capacitance λ_{cap} that can be defined as

$$\lambda_{cap} = \frac{C_a}{C_0} = \frac{l_{tot} - l_{AR}\lambda_{AR}}{l_{tot} - l_{AR}} \tag{6}$$

Equation (6) shows that by applying voltage across the AR, the increase in the mechanical strain λ_{AR} causes a decrease in the capacitive strain λ_{cap} (i.e. decrease in measured capacitance). This equation also shows the linear relationship between the capacitive strain in the SR and mechanical strain in the AR, which is ideal for implementing linear controllers.

In order to understand fully the proposed sensing mechanism, one extreme case to consider would be that with the SR placed adjacent to the AR, in which the deformation of the SR is also affected by the lateral expansion of the AR. It is assumed that in direction 1 the sensing strain remains as in equation (1), while in direction 2 the SR is stretched by the AR as

$$\lambda_{SR-L} = \lambda_{AR-L} \tag{7}$$

where λ_{AR-L} is the actuation strain of the AR in direction 2. As a result, recalling the incompressibility of the elastomer, the resulting strain in thickness becomes

$$\lambda_h = \frac{1}{\lambda_1 \lambda_2} = \frac{1}{\lambda_{SR}\lambda_{AR-L}} \tag{8}$$

Substituting equation (8) into (4), (5) and (6) yields

$$\lambda_{cap} = \frac{C_a}{C_0} = (\lambda_{SR}\lambda_{AR-L})^2 \tag{9}$$

Substituting equation (1) into (9) gives the new correlation between the capacitive strain λ_{cap} and the actuation strains λ_{AR} and λ_{AR-L} as

$$\lambda_{cap} = \frac{l_{tot}{}^2 \lambda_{AR-L}{}^2 - 2l_{tot}l_{AR}\lambda_{AR}\lambda_{AR-L}{}^2 + l_{AR}{}^2\lambda_{AR}{}^2\lambda_{AR-L}{}^2}{l_{tot}{}^2 - 2l_{tot}l_{AR} + l_{AR}{}^2}$$

$$\tag{10}$$

When the uniaxial pre-strain is relatively low (<1.5), it is expected that $\lambda_{AR} \approx \lambda_{AR-L}$, which yields

$$\lambda_{cap} = \frac{l_{tot}{}^2 \lambda_{AR}{}^2 - 2l_{tot}l_{AR}\lambda_{AR}{}^3 + l_{AR}{}^2\lambda_{AR}{}^4}{l_{tot}{}^2 - 2l_{tot}l_{AR} + l_{AR}{}^2}$$

$$\tag{11}$$
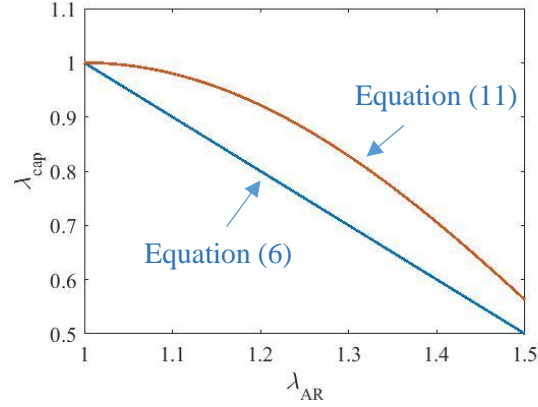
Figure 2. Comparison between the sensing mechanisms from equations (6) and (11).

Figure 2 shows that when the SR is adjacent to the AR, the deformation-capacitance correlation becomes a 4-th order polynomial as in equation (11) and has a smaller overall capacitive variation. As the SR is located further away from the AR and is less affected by its lateral expansion, the curve shifts downwards and becomes linear as in equation (6). The inhomogeneous thickness is another factor that affects the sensing. Under actuation, the deformation of the AR increases locally the thickness of the surrounding region, which would further lower the capacitive change as in equation (11). Because the lateral expansion and the inhomogeneous thickness degrades the sensing performance of the SR, it is beneficial to locate the SR away from the AR.

For comparison, in a conventional self-sensing DEA the capacitive sensing and actuation share the same AR and the correlation between them is given as

$$C_a = C_0 \frac{\lambda_A}{1/\lambda_A} = C_0 {\lambda_A}^2 \tag{12}$$

where λ_A is the ratio of the area of the actuated AR to that of the pre-strained AR. In the case of a linear actuator with full constraint in the lateral direction, because the AR deforms only in one direction, the correlation between the actuation stretch λ_{AR} and the capacitive change is derived to be quadratic as ([46])

$$C_a \propto {\lambda_{AR}}^2$$

In another case of a circular actuator, the correlation between the actuation strain in radial direction λ_r and the capacitive change holds as ([10])

$$C_a \propto {\lambda_r}^4$$

Such high-order correlations amplify noise in the associated capacitive measurement signals and limit the use of standard linear PID control action. More sophisticated control algorithms are therefore required to achieve optimal performance. Furthermore, because the SR in the DESA senses only the deformation in the single direction, the planar expansion of the AR is decoupled and can be measured separately for each direction. Such a sensing mechanism is more informative and beneficial in controlling more complex DEA-based systems. In the case when wrinkling of the elastomer occurs, the deformation of the AR is out-of-plane and it does not cause the consequential deformation of the rest of the structure. Then equation (6) is no longer applicable, and the SR does not senses the out-of-plane actuation, which also differs from the conventional self-sensing mechanism.

2.2 Force actuation in correlation to capacitive sensing
For the DESA as a force actuator, the equation of state in direction 1 is given by

$$\sigma_1 + \varepsilon E^2 = \frac{\lambda_1 \partial W(\lambda_1, \lambda_2)}{\partial \lambda_1} \tag{13}$$

where σ_1 is the stress due to the mechanical loading, εE^2 is the stress due to the electrical loading and $W(\lambda_1, \lambda_2)$ is the elastic free energy density function of the elastomer in terms of the in-plane strains λ_1 and λ_2. When the DE is pre-loaded only, σ_1 can be solved as the resultant mechanical stress by setting $E = 0$, The stress differences between the actuated and pre-loaded states contributes to the force output of the DESA as

$$\Delta\sigma_1 = -\varepsilon E^2 \tag{14}$$

With the assumption of small voltage-induced deformation across the elastomer with strains up to 20%, the elastic modulus, Y_1, in direction 1 is assumed to remain constant throughout the operation. The net stress $\Delta\sigma_1$ can be correlated to λ_{AR} as

$$\Delta\sigma_1 = Y_1(\lambda_{AR} - 1) \tag{15}$$

Substituting equation (6) into (15) and taking the cross-sectional area of the elastomer into account, the force output of the DESA, ΔF, can be expressed as

$$\Delta F = whY_1\left(\frac{l_{tot}}{l_{AR}} - 1\right)(1 - \lambda_{cap}) \tag{16}$$

Equation (16) shows that the force output is proportional to the capacitive strain. The linear correlation is also beneficial for the implementation of linear controllers.

(a)   (b)   (c)
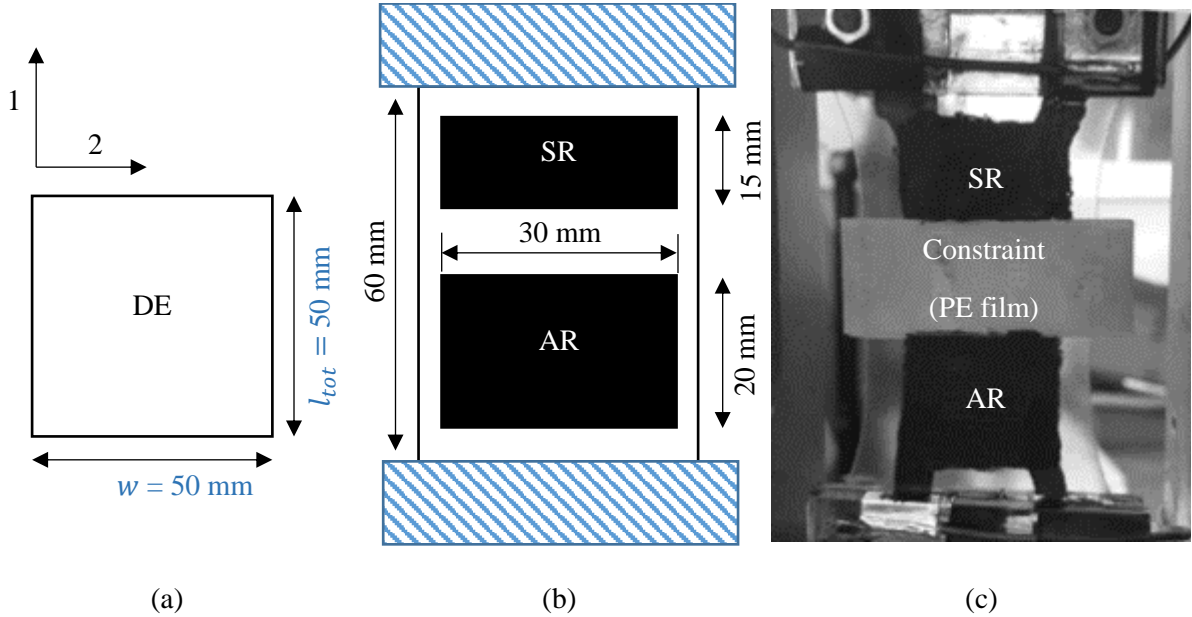
Figure 3. The configurations of the DESA: (a) the original DE film, (b) the pre-strained DE with electrode coating and (c) the actual DESA that is further enhanced with the motion-constrained layer.
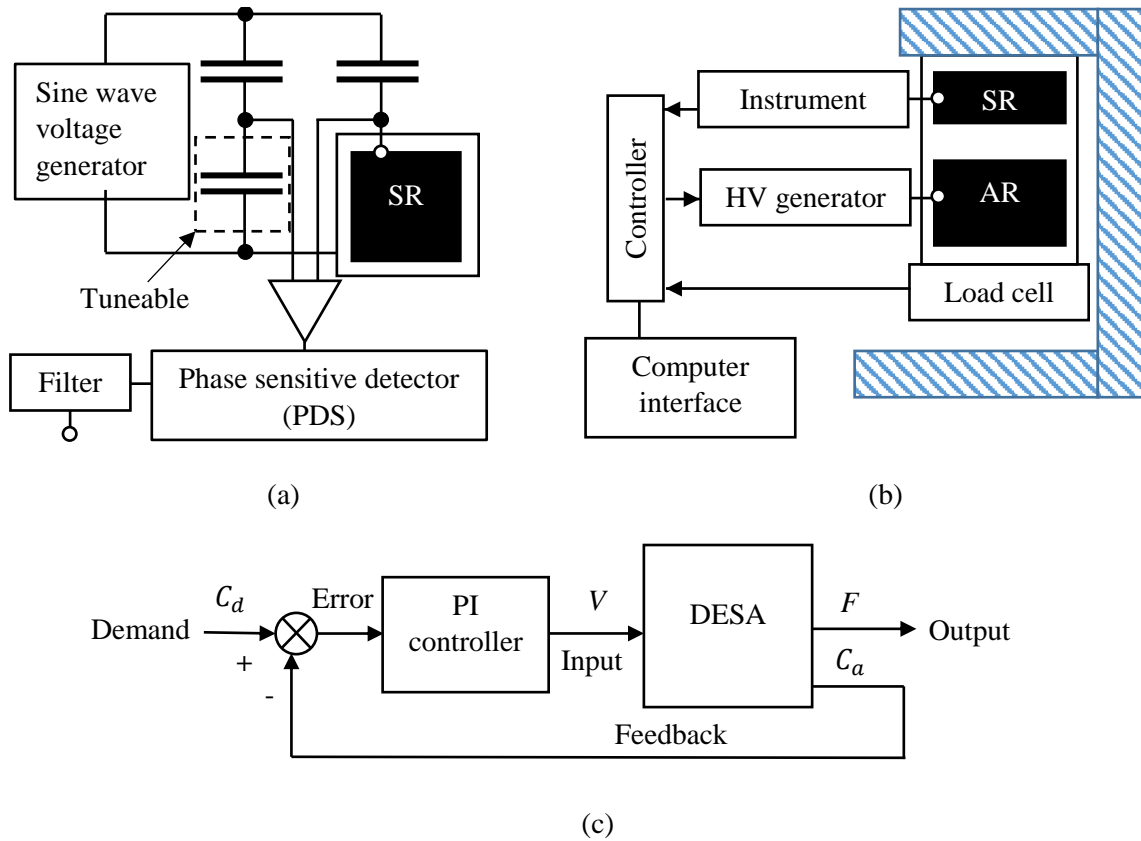
Figure 4. Schematic diagrams of (a) the capacitor-bridge-based instrument for capacitive measurement, (b) the experimental setup and (c) block diagram for closed loop operation.

3. Experimental Setup

The structure of the DESA is configured as shown in figure 3. The DE used in this work is the polyacrylate VHB 4910 from 3M. The 1 mm thick tape was laser cut into the square of 50 mm × 50 mm (figure 3a). After that the DE was pre-strained by $\lambda_{1,pre} = 50\%$, and the electrode was applied according to figures 3b and 3c. For the electrode regions, the SR was 15 mm × 30 mm and the AR was 20 mm × 30 mm. The applied electrode material was carbon black grease from MG, which was brushed onto the DE. The AR and the SR were aligned in direction 1 and the gap in between them was set to be 15 mm to reduce any signal noise transmission due to the high electric field during the capacitive measurement. A layer of the PE film was also applied onto this gap to improve further the sensing and actuation conditions of the DESA.

The test rig setup is shown in figure 4b. The pre-strained DE was held by two clamps (figure 3c) that were made from acrylic material. Aluminium tape was wrapped around each clamp to provide the electrode contact. The top clamp connects the SR to the instrument for the capacitive sensing; the bottom clamp connects the AR to the HV generator for the actuation. On the bottom, the DE was mounted to a load cell for the force measurement up to 2 N. A HV generator was able to apply voltages up to 15 kV. With appropriate scaling, the actual voltage output was monitored in the range 0-10 V. An instrument was designed to measure the capacitance in pF with the resolution of 0.001 pF. The capacitive measurement was achieved by using the capacitor bridge arrangement shown in figure 4a. The instrument contained three capacitors, one of which was tuneable. Along with the SR in the DESA, they form a capacitor bridge. A sensing signal at 10 kHz was generated and inputted to the capacitor bridge. In operation, the SR deforms, and its capacitance changes. As a result, the voltage difference between two pairs of capacitors was measured via a differential amplifier and calibrated to represent the capacitive measure.

For the basic characterization of the DESA, the system was actuated with a sequence of step up/down voltages and the force and the capacitance measurements were monitored. To compare the open and closed loop operations of the DESA, the reference was set to be a step change in the capacitance between the two arbitrarily chosen values, 28.60 pF and 28.55 pF. Each test lasted for 23 s with the voltage applied from $t = 3$ s. In open-loop operation, the voltage was applied as a step input and its value was pre-determined from prior testing. The closed loop operation of the DESA is explained in figure 4c. It is intended to use the error, $E(s)$, between the demand capacitance, $C_d(s)$ and the actual capacitance state, $C(s)$, as the feedback to control the Laplace transformed force output, $F(s)$. The PI controller is defined as

$$G(s) = \frac{V(s)}{E(s)} = K_p + K_i \frac{1}{s} \qquad (17)$$

where

$$E(s) = C_d(s) - C(s) \qquad (18)$$

The gains, K_p (V/pF) and K_i (V/pF/s), were tuned iteratively so that when subjecting a step demand of $C_d(s)$, the response in $C(s)$ has a rise time less than 0.5 s and the overshoot is less than 10%. A standard PI controller (K_p = 10 V/pF and K_i = 2 V/pF/s) was used to vary the applied voltage according to the feedback of the capacitance signal. Noting that the control is applied to the capacitance output, for a viscoelastic DE such as polyacrylate, demanding a fast capacitive response also causes significant overshoot in the force output.

4. Results and discussion

### 4.1 Closed loop control in force operation

Figure 5a shows the step responses of the DESA. The test lasted for 200 s with the applied voltage switching between 0 kV and 8 kV, where the voltage is supplied for 10 s in each cycle of 20 s. It shows that the voltage application corresponds to a relaxation of the DE and decrease in the capacitance in

(a)   (b)
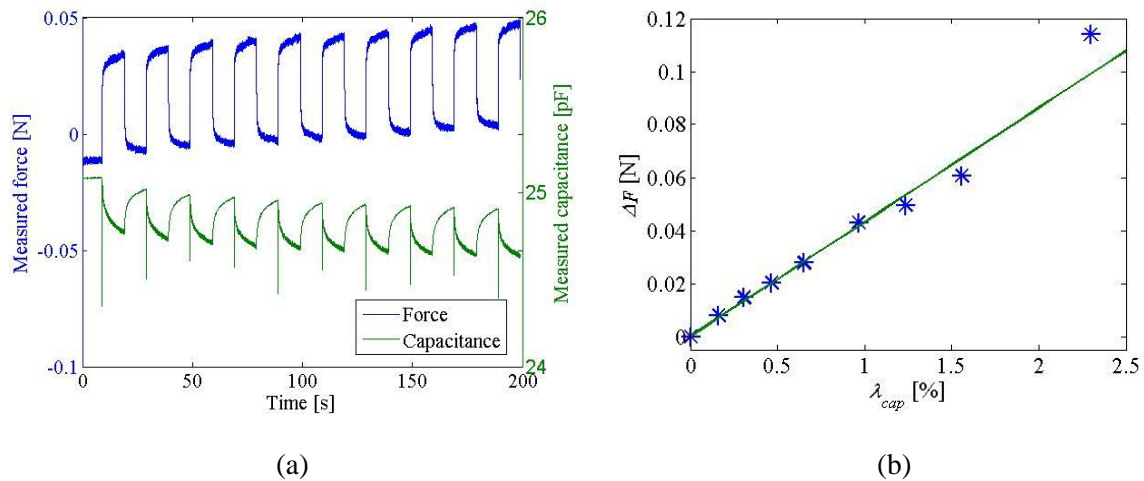
Figure 5. The system responses of the DESA: (a) The step responses of force and capacitance at 8 kV, the spikes in the capacitance are due to interference of the strong electrical field when switching on the HV DC-DC converter at the beginning of each cycle. (b) The net force output against the strain in capacitance with the applied voltage from 3 kV to 11 kV in increment of 1kV. The linear correlation is in agreement with equation (16).

both the long-term and the short-term responses. Over 200 s, the tension force of the pre-strained DE dropped by 0.015 N and the capacitance of the SR dropped by 0.2 pF. In each loading cycle of 10 s, the steady state outputs of the force and the capacitance were calculated between $t = 9.5$ s, just before the voltage application and at the end, $t = 20$ s. Figure 5a shows the step change force output of the DESA was 0.044 N, and the capacitive change was 0.25 pF. For the dynamics of the response, an instant drop of 90% followed by a slow decrease was observed in the force; the corresponding drop was observed as 50% in the capacitance, indicating that the force status responds significantly faster than the capacitance status due to the strong viscoelasticity of the polyacrylate. Figure 5b summarizes the net force output of the DESA, F, and the corresponding capacitive strain, λ_{cap}, under the applied voltage of 3 kV to 11 kV. At 11 kV, the actuation generates the force of 0.115 N and the capacitive strain of 2.4%. The relationship between these two outputs were found to be linear, which is in agreement with equation (16). Therefore it indicates that in such electrode arrangement, the capacitive change of the SR only correlates the actuation-induced deformation in a single direction.

Figure 6 compares the results of the both operations. In closed loop operation, the applied voltage rises to 8.5 kV and then decreases slowly to 5.5 kV as in figure 6a. In open-loop operation, the applied voltage rises from 3 kV to 7 kV and remains constant. The measured capacitance in the case of closed loop operation decreases immediately from 28.6 pF to 28.55 pF within 0.5 s; in open-loop operation, it creeps from 28.6 pF towards 28.55 pF over 3 s and continues to decrease towards 28.5 pF as in figure 6b. The measured force in the case of the closed loop operation has an overshoot of 0.013 N at $t = 3$ s,


(a)

(b)

(c)
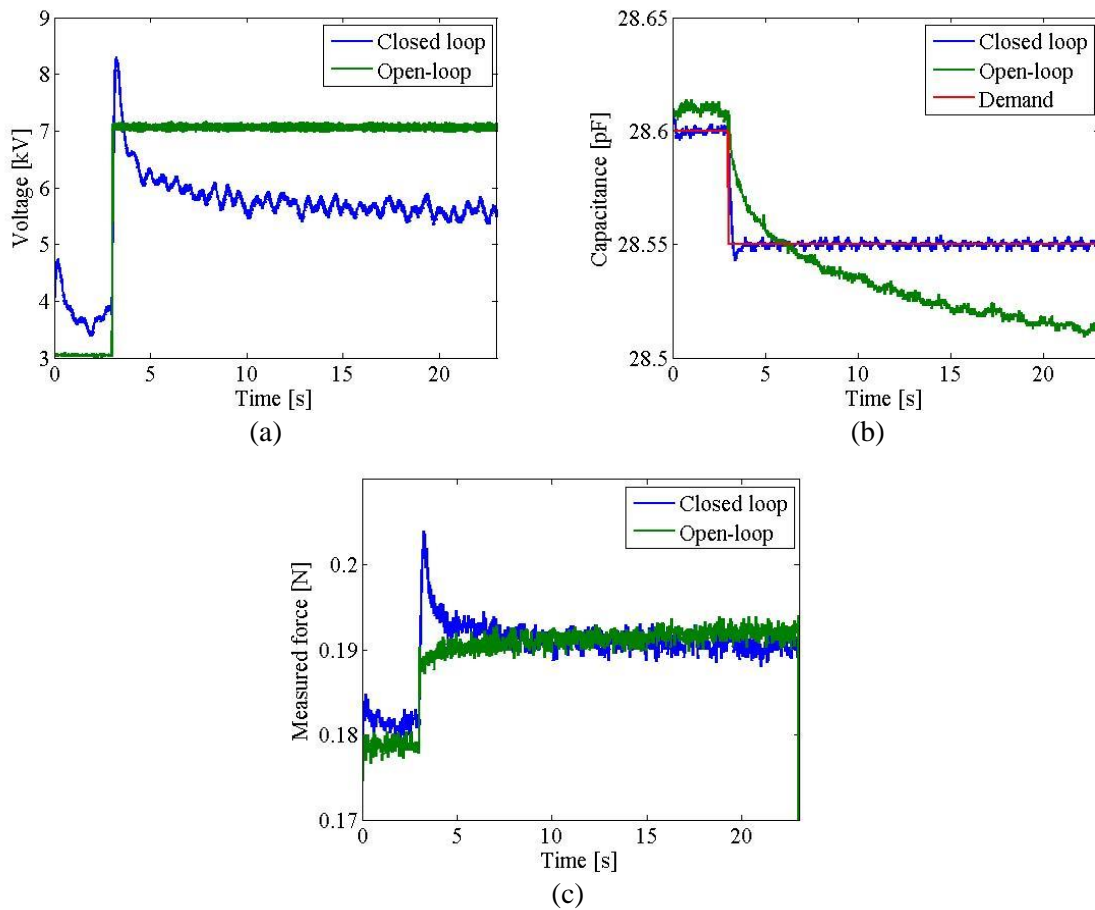
Figure 6. System responses in open-loop and closed loop operations (a) the voltage input, (b) the measured capacitance and (c) the measured force.

it reaches the steady state of 0.19 N and holds in this value from $t = 5$ s. For the open-loop operation, the measured force has an initial rise of 0.01 N and reaches 0.19 N at $t = 10$ s, after which point it continues to increase throughout. The result shows that closed loop operation allows the DESA to react more quickly and suppresses the creeping effects in the capacitive and the force outputs. However, because the polyacrylate is strongly viscoelastic, in order to achieve rapid deformation (e.g. actuation strain), a higher initial voltage is required to deliver a large driving force. As a result, an overshoot of approximately 100% in the force output is observed in figure 6c. The force-capacitance correlation in equation (16) represents only the steady state of the actuation because equation (15) does not include rate-dependency. Therefore the overshoot and the dynamics of the actuation are not predicted by the derived correlation. In contrast, for elastomers such as silicone that behave elastically, because the rate-dependent effect is negligible, the overshoot in the actuation force in such closed loop operation becomes significantly smaller and equation (16) holds true for both the dynamic and steady states of the actuation.

4.2 Drifting effect in capacitance-strain correlation

Rosset *et al*. [43] reported that in the position control of the conventional self-sensing DEA, an unexpected drift in the capacitance-strain relationship was reported in the DEA that is made of the polyacrylate. In this work, the self-sensing mechanism was applied in controlling a tuneable grating. A rectangular DE was pre-strained and clamped on a rigid frame with the two electrode regions and equipped with a soft grating in the centre. Both of the electrode regions were used for sensing and actuation; the capacitive sensing was used as a feedback for precise control in the deformation of the structure. Given that, the grating was controlled without requiring external sensors. The results showed promising performance in the grating control with standard linear PI controller, despite of the nonlinear relationship between the diffraction angle in the grating and the capacitance of the electrode regions. Rosset *et al*. [43] also reported that in the polyacrylate-based DEA structure, while the capacitance was held by the closed loop operation, the diffraction angle continues to drop over 400 s. It indicates that the DE relaxes in the long-term and such relaxation is independent of the capacitance of the electrode regions. Further investigation in this work showed that such drift occurred only in the viscous elastomer as the polyacrylate compared with silicone. It was concluded that the drift in the capacitance-strain relationship was due to the rate-dependent behaviour of the permittivity of the polyacrylate when it is subjected to a high electric field.

The same investigation was carried out in the DESA. Figure 7 shows the results of the force and the capacitance over 500 seconds. From $t = 50$ s, the voltage was applied to the AR with the closed loop control. It shows that the capacitance reached the demand value instantly thanks to the PI controller.
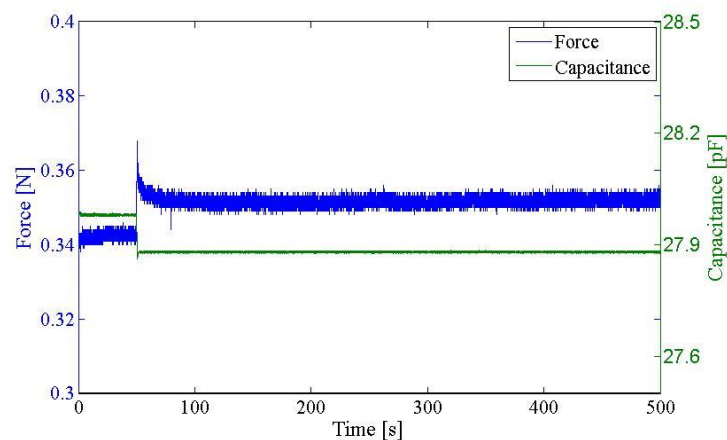

Figure 7. Closed loop operation on the DESA over 500 s for the inspection of the potential drifting in capacitance-strain relationship.

The force rose correspondingly with an overshoot and settled down within 20 s before reaching the steady state at $t = 70$ s. It shows no drift in the capacitance-strain relationship has occurred after this point. The duration of settlement is significantly shorter than that of 400 s in [43], which arises since no high electric field is applied directly across the SR during operation. Therefore the rate-dependent behaviour in the permittivity did not occur. The result shows good agreement with the conclusion from [43] and highlights another benefit of the DESA compared with the conventional self-sensing DEA. Because separate electrode regions were used for the actuating and the sensing, the potential high-electric-field-induced dynamics in the material property would not interfere the measurement in capacitance; the DESA is more robust and consistent in the high-voltage DE actuation.
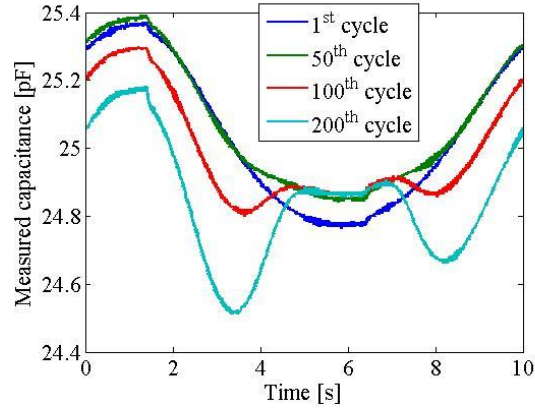
4.3 Effect of the electrode

In the AR, the electrode coverage affects the voltage-induced deformation. Since the hand-brushed grease electrode has good compliance with the deformation it tends to provide better actuation performance compared with the hand-painted powder type electrode. Similarly, the particle size of powder type electrode also has impact on the DEA actuation. A non-uniformly distributed electrode may cause concentration of charge and lead to the electrical breakdown. The resultant deformation occurs in different levels correspondingly and the profile of the response remains the same throughout. Even when the electrode is poorly coated over the AR, the high operating voltage helps the charge to cross potential gaps and the DEA is still functional.

In contrast, the capacitive sensing was found to depend heavily on the quality of the electrode arrangement. Since controlling the thickness of the electrode is difficult, as indicated in [47], a study was undertaken to investigate the effect of electrode coverage in the capacitive measurement in the undeformed condition. All configurations of the DESA remained the same in this study, the electrodes were painted onto the SR accumulatively over many coating applications from barely covering the whole region to an excessively thick layer (above 1 mm). For each application, approximately the same amount of the additional electrode was added onto both sides of the SR. The applications of electrode addition were continued until the measured capacitance stopped varying significantly. Figure 8 shows the capacitance measurement over 25 applications. The measured capacitance was 24.4 pF at the first application. It then continued to rise as more electrode material was accumulated on the SR, and finally
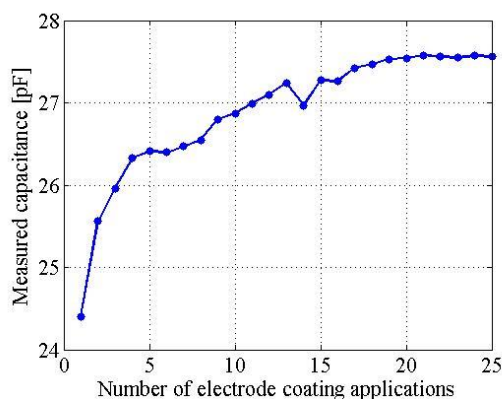
Figure 8. The statistics of the capacitive measurements under the electrode coverage that is accumulated over 25 applications.

Figure 9. The capacitive responses of the DESA under cyclical strain, the profile deviates from the sinusoidal curve over cycles due to the defect propagation in the electrode coating.

approached 27.5 pF at the 25th application. There is up to 12% variation in the capacitance over 25 applications, half of which occurred within first three applications. This indicates that the electrode coating over multiple applications is beneficial in achieving consistent capacitance, especially with the grease-type of electrode.

Moreover, the work also found that the electrode migration changes the profile of the capacitive response. As the DE undergoes deformation over a period of time, the electrode was found to reveal that unexpected spots that contain less electrode material existed across the SR. These spots do not exist when the electrode is coated on the DE. It indicates the presence of defect propagation in electrode coating due to the particle migration in the SR. The study was done by performing sinusoidal loading on the DE and monitoring its capacitance throughout. The structure was simplified to have only the SR in the DE. The cyclic strain was set to strain the film from 50% pre-strained to 60%. The electrode coverage was done to assure the sinusoidal response at the beginning of the test. Figure 9 shows the degradation in the capacitive profile as the response no longer remains sinusoidal over cycles. The multiple troughs started to appear after 100 cycles of strain and continued to propagate thereafter. Such testing was done over multiple samples, the unexpected profiles in the capacitive responses were similar but not identical. Also, the occurrence of the degradations varied and depended on the configurations of the electrode (e.g. layer thickness and uniformity). It indicates that electrode migration occurs in the small deformation regions. Despite the full understanding of the electrode defect propagation requires further work, an effective solution was to make the electrode layer thicker. It was found experimentally that using a screen to provide the more consistent electrode coating and having the electrode layer of at least 0.3 mm thick ensures the consistent capacitive response over 800 cycles. It also gives the consistent capacitive measurement in the DESA.

4.4 Effect of AR-SR aspect ratio
The correlation between the sizes of the SR and the AR also affects the performance of the DESA. By keeping the shape and the width of electrode regions the same, the aspect ratio R of the SR and the AR is defined as

$$R = \frac{l_{SR}}{l_{AR}} \tag{19}$$

Hence the overall length of the film l_{tot} can be expressed as

$$l_{tot} = (1 + R + R_d)l_{AR} \tag{20}$$

where $R_d l_{AR}$ refers to the part of the film without electrode region in direction 1. Substituting equation (20) into (6) gives

$$\lambda_{cap}(\lambda_{AR}) = 1 + \frac{1}{R+R_d} - \frac{\lambda_{AR}}{R+R_d} \qquad (21)$$

The sensing sensitivity of the DESA is defined as

$$S = \frac{\partial \lambda_{cap}}{\partial \lambda_{AR}} = -\frac{1}{R+R_d} \qquad (22)$$

Equation (22) shows that the sensing sensitivity can be improved by decrease both R and R_d (i.e. enlarge the AR in relative to the passive region and SR). It also benefits the actuation capability of the DESA since having the SR does not require to compromise the size of the AR.

Theoretically, the sensing sensitivity can be optimized by having the significantly high aspect ratio. However, the actual lower limit of R depends on the instrument for the capacitive measure as indicated in equation (4). As the area of the SR becomes smaller, the capacitance of the SR decreases and becomes more difficult to measure as it approaches the level of the noise. The capacitor bridge was developed for the capacitive measure in pF precisely. The trade-off is that it is also very sensitive to the noises from the environment. The actual lower limit of R_d depends on the spacing gap between the AR and the SR. When the DESA is in operation, electrical breakdown is the primary concern in determining the gap distance. If breakdown occurs, the high voltage from the AR causes arcs onto the SR, which interferes with the capacitive measure and damages the instrument. Therefore the breakdown strength of the environment (i.e. air in this case) must be considered. Moreover, the strong electrical field from the AR fluxes through both the elastomer and the environment. As the SR lays closer to the AR, such unexpected electrical field is received by the SR and interferes the capacitive measurement as shown in figure 5a. The noise level increases when the voltage is applied. In this work for DEA operating in the air, the gap distance of 15 mm was found to be safe for the applied voltage up to 15 kV.

4.5 Effect of motion-constraining

While the passive region between the electroded regions arises from necessity, the constraints can be applied to further enhance the sensing sensitivity of the DESA. By constraining the deformation of the passive region, the voltage-induced expansion in the AR corresponds to the larger compression in the SR, therefore higher sensing sensitivity. Since this part of the DE no longer deforms during the operation, the effect of such motion-constraint can be expressed as a decrease in R_d in equation (22). The remaining passive region would be those between electrode regions and clamps, which could constrained similarly. In the ideal case, all the passive regions in the DE are fixed in dimension as $R_d = 0$, substituting it into equation (22) gives

$$S = \frac{\lambda_{cap}}{\lambda_{AR}} = -\frac{1}{R} \qquad (23)$$

(a)   (b)
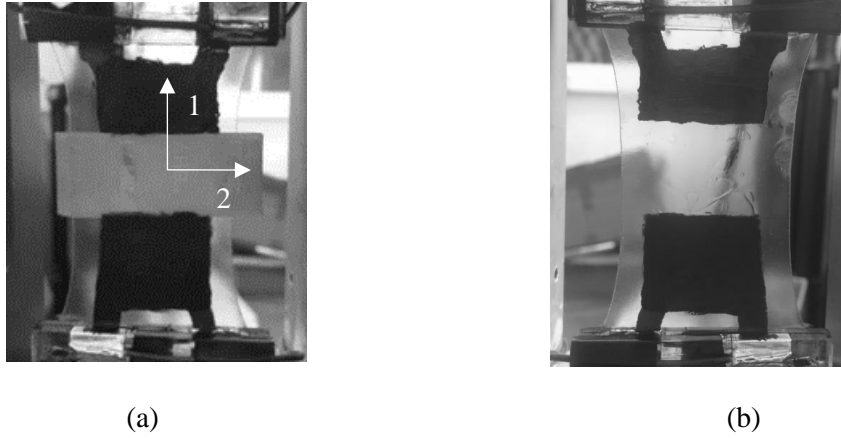
Figure 10. The actual DESAs (a) with constraint and (b) without constraint.

(a)   (b)
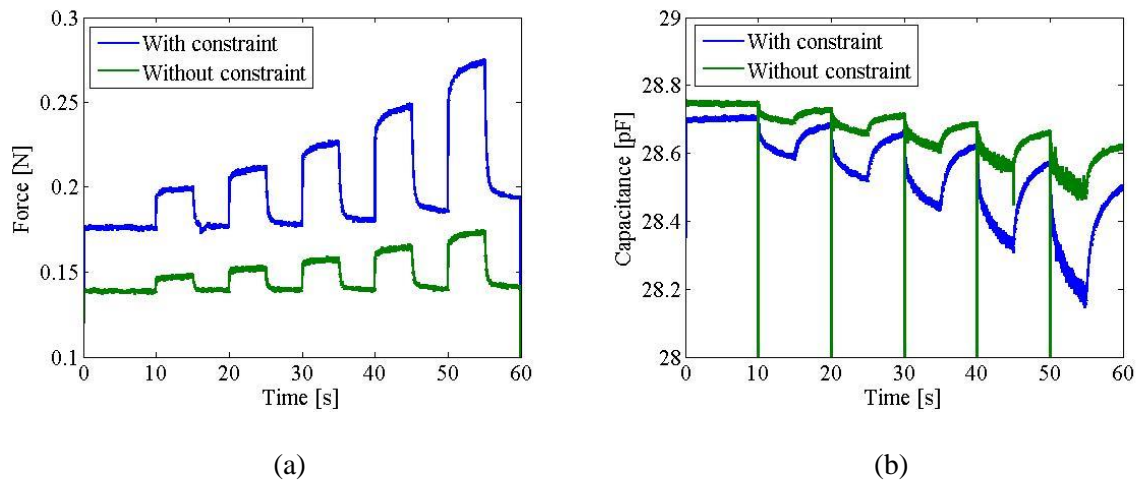
Figure 11. Comparison between the DESAs with and without constraint (a) force response and (b) capacitance response.

Equation (23) indicates that the sensitivity S depends solely on R and becomes more sensitive to the change in R, correspondingly. Furthermore, applying such constraint to the DE also enhances actuation performance in the AR by constraining its expansion in direction 2 [48].

Figure 10 shows the actual DESA in the unconstrained and constrained conditions. Figures 11a and 11b shows that the force and capacitance responses of the DESA under the step voltage input from 6 kV to 10 kV. The improvement in the outputs due to the motion-constraint was by a factor of 3. In this work, a layer of the PE film was used to serve the purpose without compromising the flexibility of the DESA. However, such a flexible constraint requires the careful application so that the constrained passive region remains in-plane. The curvature and the misalignment vary the capacitance-strain relationship and cause errors in sensing. Finally, the employed constraint is required to be as light as possible so that the additional mass does not result in the undesired resonance and interferes the system dynamics significantly.

4.6 Wrinkling detection of the DESA
The DESA shows the promising performance when the AR undergoes deformation strains up to 10%. Recalling the stress-strain relationship of a typical DE, the snap point in the stress-strain curve is delayed as the DE is pre-strained [5]. Such change in the material property allows the DE to deform significantly larger under the same applied voltage without the electrical breakdown [7]. Because the resultant local

strain in the AR becomes excessive, it causes the out-of-plane deformation in the AR, namely the wrinkling. The relationship between the capacitive strain in the SR and the mechanical strain in the AR as in equation (6) differs as the result.

Regarding this, a study was done to investigate the sensing limitation of the DESA against the voltage-induced wrinkling. To do so, a DE was pre-strained bi-axially with $\lambda_{1,pre} = 2$, $\lambda_{2,pre} = 2$ and mounted on a rectangular rigid frame. The AR is 15 mm $\times$ 50 mm and the SR is 10 mm $\times$ 10 mm. The SR was designed to be relatively small and aligned with the AR in direction 1 so that the SR senses the largest local deformation of the central AR. Copper foils were wrapped on the frame for the electrode contract. The voltages were applied to the DESA as step inputs for 2 s from $t = 1$ s, the capacitance was monitored for 5 s in each test. In order to cause wrinkling within the achievable input voltage, the DESA was pre-strained equally in both directions to lower further the thickness of the film. Changing the pre-loading condition varies only actuation strains in planar directions [49]. Equations (1), (3), (6) and (16) therefore still holds in the equal-biaxial loading condition.

Figure 12 shows the capacitive responses that are associated with wrinkled actuation at different voltages. At 1 kV, the capacitance reached the steady state within 0.1 s at $t = 1$ s. At $t = 3$ s, the capacitive response rises back over 0.5 s. At 4 kV, it took 0.5 s for the capacitance to reach the steady-state when activating the AR, and over 1 s to recover from the actuation from $t = 3$ s. It shows that as the voltage increases further, the capacitance takes longer to reach the steady state and its static output approaches a saturation value. In the experiment, it was observed that the wrinkling occurred initially in direction 2 at 5 kV, indicating excessive strain only in direction 1. As the voltage increased further, the wrinkling became prismatic as it propagated in both planar directions as in figure 13. Either way, it causes the additional lag in recovering from the wrinkled actuation. During the recovery, the geometry of the SR remains unaffected, in which case the large deformation in the AR can no longer be detected by the capacitive change in the SR. For example, the more significant wrinkling occurred at 7 kV and took over 2 s to recover; the measured capacitive change of 1 pF remains the same as that at 6 kV. Therefore, the two features of:

A1. Capacitive change stops increasing when increasing the applied voltage (e.g. the saturation in capacitance)

A2. Capacitive change decreases with a significant time delay when decreasing the applied voltage (e.g. significant time delay).

This makes the DESA provide informative feedback about wrinkling, which can be used for holding the actuation within the in-plane state to avoid the potential failure.
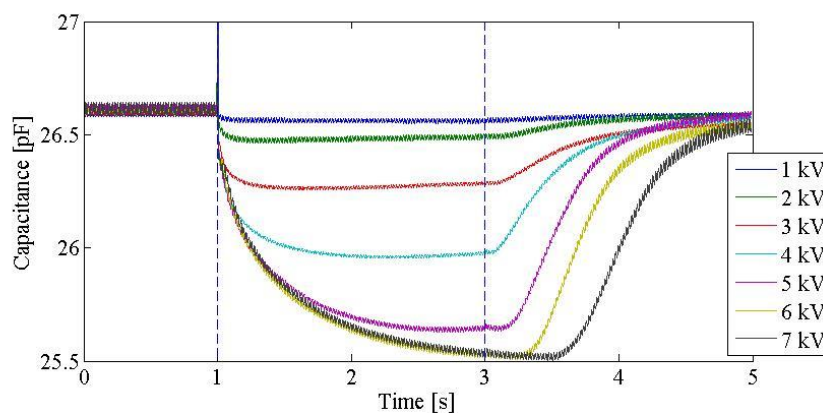
Figure 12. The step responses of the actuation in the largely pre-strained DESA that is associated with the occurrence of the out-of-plane deformation.

(a)   (b)
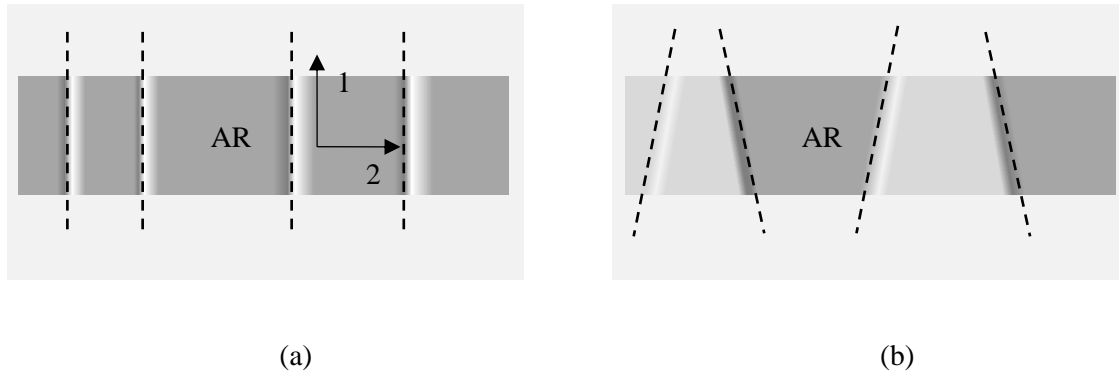
Figure 13. Illustration of the change in the wrinkling as the applied voltage increases: (a) Wrinkling occurs only in one direction and is aligned in direction 1 at 5 kV and (b) At higher applied voltage (> 5 kV), the wrinkling occurs in both planar directions and forms prismatic sub-regions.

5. Conclusions

In this work, the structure of a new DESA design is proposed that features a self-sensing mechanism. Compared with a conventional self-sensing DEA, the DESA consists of multiple electrode regions for sensing and actuation. In operation, the voltage is applied on the AR for actuation, and the capacitance of the SR is measured and used as feedback in the force control. Because of this, the sensing by the SR detects only the deformation of the structure in a single direction. An instrument based on a capacitor bridge was designed for the capacitive measurement. For a step input of voltage in kV, the resultant capacitive change was measured on the scale of 0.1 pF. In the polyacrylate-based DESA, the closed loop operation shows the promising performance in achieving the fast response and suppressing the relaxation. The drawback in achieving rapid response in the capacitance is that it also causes an overshoot in force output due to the strong viscoelasticity of the polyacrylate.

For the electrode coating of the DESA, the capacitive measurement is very sensitive to the electrode coverage in the SR for the grease type electrode. Without the high electric field, good conductivity is necessary for the charges to spread across the entire SR. Poor electrode coverage and defects in electrode coating lead to the unexpected capacitive response. Increasing the thickness of the electrode layer is one option to improve the electrode coverage effectively. Also, it shows that the performance of the DESA can be further enhanced by:

    B1. Varying the aspect ratio of the electrode regions
    B2. Utilizing motion-constraint.

These factors benefit both the sensing and the actuation of the DESA. Furthermore, the study shows that the DESA structure does not suffer from the rate-dependent permittivity due to high electric field compared that was observed in the conventional self-sensing DEA. It makes the DESA operate more consistently over a broad range of operating voltage. Finally, the DESA shows distinct capacitance responses between linear and the nonlinear actuation, which can be exploited for detecting the excessive local strain in the AR.

Reference

1. Carpi, F.; De Rossi, D.; Kornbluh, R.; Pelrine, R. *Dielectric elastomers as electromechanical transducers*. 2008.
2. Li, T.; Zou, Z.; Mao, G.; Qu, S. Electromechanical bistable behavior of a novel dielectric elastomer actuator. *Journal of Applied Mechanics, Transactions ASME* **2014**, *81*.
3. Li, T.; Li, C.; Mao, G.; Zou, Z.; Xie, Y.; Qu, S. In *Novel dielectric elastomer structures with electromechanical instability*, Proceedings of SPIE - The International Society for Optical Engineering, 2014.
4. Li, T.; Li, W.; Zou, Z.; Hong, Z.; Qu, S. Effects of stretching rate and size on the rupture of acrylic dielectric elastomer. *International Journal of Applied Mechanics* **2014**, *6*.
5. Mao, G.; Li, T.; Zou, Z.; Qu, S.; Shi, M. Prestretch effect on snap-through instability of short-length tubular elastomeric balloons under inflation. *International Journal of Solids and Structures* **2014**, *51*, 2109-2115.
6. Zou, Z.; Li, T.; Qu, S.; Yu, H. Active shape control and phase coexistence of dielectric elastomer membrane with patterned electrodes. *Journal of Applied Mechanics, Transactions ASME* **2014**, *81*.
7. Li, T.; Keplinger, C.; Baumgartner, R.; Bauer, S.; Yang, W.; Suo, Z. Giant voltage-induced deformation in dielectric elastomers near the verge of snap-through instability. *Journal of the Mechanics and Physics of Solids* **2013**, *61*, 611-628.
8. Li, T.; Qu, S.; Yang, W. Electromechanical and dynamic analyses of tunable dielectric elastomer resonator. *International Journal of Solids and Structures* **2012**, *49*, 3754-3761.
9. Mannsfeld, S.C.B.; Tee, B.C.K.; Stoltenberg, R.M.; Chen, C.V.H.H.; Barman, S.; Muir, B.V.O.; Sokolov, A.N.; Reese, C.; Bao, Z. Highly sensitive flexible pressure sensors with microstructured rubber dielectric layers. *Nature Materials* **2010**, *9*, 859-864.
10. Jung, K.; Kim, K.J.; Choi, H.R. A self-sensing dielectric elastomer actuator. *Sensors and Actuators, A: Physical* **2008**, *143*, 343-351.
11. Liu, Y.; Liu, L.; Zhang, Z.; Jiao, Y.; Sun, S.; Leng, J. Analysis and manufacture of an energy harvester based on a mooney-rivlin-type dielectric elastomer. *EPL* **2010**, *90*.
12. Lv, X.; Liu, L.; Liu, Y.; Leng, J. Dielectric elastomer energy harvesting: Maximal converted energy, viscoelastic dissipation and a wave power generator. *Smart Materials and Structures* **2015**, *24*.
13. Li, T.; Qu, S.; Yang, W. Energy harvesting of dielectric elastomer generators concerning inhomogeneous fields and viscoelastic deformation. *Journal of Applied Physics* **2012**, *112*.
14. Anderson, I.A.; Gisby, T.A.; McKay, T.G.; O'Brien, B.M.; Calius, E.P. Multi-functional dielectric elastomer artificial muscles for soft and smart machines. *Journal of Applied Physics* **2012**, *112*.
15. Anderson, I.A.; Hale, T.; Gisby, T.; Inamura, T.; McKay, T.; O'Brien, B.; Walbran, S.; Calius, E.P. A thin membrane artificial muscle rotary motor. *Applied Physics A: Materials Science and Processing* **2010**, *98*, 75-83.
16. Brochu, P.; Pei, Q. Advances in dielectric elastomers for actuators and artificial muscles. *Macromolecular Rapid Communications* **2010**, *31*, 10-36.
17. Choi, H.R.; Jung, K.M.; Kwak, J.W.; Lee, S.W.; Kim, H.M.; Jeon, J.W.; Nam, J.D. In *Multiple degree-of-freedom digital soft actuator for robotic applications*, Proceedings of SPIE - The International Society for Optical Engineering, 2003; pp 262-271.
18. Bar-Cohen, Y. In *Biomimetic actuators using electroactive polymers (eap) as artificial muscles*, International SAMPE Symposium and Exhibition (Proceedings), 2006.
19. Jung, K.; Nam, J.; Lee, Y.; Choi, H. In *Micro inchworm robot actuated by artificial muscle actuator based on non-prestrained dielectric elastomer*, Proceedings of SPIE - The International Society for Optical Engineering, 2004; pp 357-367.
20. Pelrine, R.; Kornbluh, R.; Pei, Q.; Stanford, S.; Oh, S.; Eckerle, J.; Full, R.; Rosentha, M.; Meijer, K. In *Dielectric elastomer artificial muscle actuators: Toward biomimetic motion*, Proceedings of SPIE - The International Society for Optical Engineering, 2002; pp 126-137.
21. O'Brien, B.; McKay, T.; Calius, E.; Xie, S.; Anderson, I. Finite element modelling of dielectric elastomer minimum energy structures. *Applied Physics A: Materials Science and Processing* **2009**, *94*, 507-514.

22.   Aschwanden, M.; Stemmer, A. In *Low voltage, highly tunable diffraction grating based on dielectric elastomer actuators*, Proceedings of SPIE - The International Society for Optical Engineering, 2007.

23.   Carpi, F.; Frediani, G.; Turco, S.; De, R.D. Bioinspired tunable lens with muscle-like electroactive elastomers. *Advanced Functional Materials* **2011**, *21*, 4152-4158.

24.   Aschwanden, M.; Niederer, D.; Stemmer, A. In *Tunable transmission grating based on dielectric elastomer actuators*, Proceedings of SPIE - The International Society for Optical Engineering, 2008.

25.   Kollosche, M.; Döring, S.; Stumpe, J.; Kofod, G. Voltage-controlled compression for period tuning of optical surface relief gratings. *Optics Letters* **2011**, *36*, 1389-1391.

26.   Beck, M.; Fiolka, R.; Stemmer, A. Variable phase retarder made of a dielectric elastomer actuator. *Optics Letters* **2009**, *34*, 803-805.

27.   Pei, Q.; Pelrine, R.; Stanford, S.; Kornbluh, R.; Rosenthal, M.; Meijer, K.; Full, R. In *Multifunctional electroelastomer rolls and their application for biomimetic walking robots*, Proceedings of SPIE - The International Society for Optical Engineering, 2002; pp 246-253.

28.   Jordi, C.; Michel, S.; Kovacs, G.; Ermanni, P. Scaling of planar dielectric elastomer actuators in an agonist-antagonist configuration. *Sensors and Actuators, A: Physical* **2010**, *161*, 182-190.

29.   Sarbana, R.; Oubaeka, J.; Jones, R.W. In *Closed-loop control of a core free rolled eap actuator*, Proceedings of SPIE - The International Society for Optical Engineering, 2009.

30.   Sarban, R.; Jones, R.W. In *Physical model-based internal model control of a de actuator*, Proceedings of SPIE - The International Society for Optical Engineering, 2011.

31.   Randazzo, M.; Fumagalli, M.; Metta, G.; Sandini, G. In *Closed loop control of a rotational joint driven by two antagonistic dielectric elastomer actuators*, Proceedings of SPIE - The International Society for Optical Engineering, 2010.

32.   Kaal, W.; Herold, S. Electroactive polymer actuators in dynamic applications. *IEEE/ASME Transactions on Mechatronics* **2011**, *16*, 24-32.

33.   O'Brien, B.; Thode, J.; Anderson, I.; Calius, E.; Haemmerle, E.; Xie, S. In *Integrated extension sensor based on resistance and voltage measurement for a dielectric elastomer*, Proceedings of SPIE - The International Society for Optical Engineering, 2007.

34.   Gisby, T.A.; O'Brien, B.M.; Anderson, I.A. In *How far and how hard: Tactile feedback for robotic manipulators*, Proceedings of SPIE - The International Society for Optical Engineering, 2012.

35.   Gisby, T.A.; Xie, S.; Calius, E.P.; Anderson, I.A. In *Integrated sensing and actuation of muscle-like actuators*, Proceedings of SPIE - The International Society for Optical Engineering, 2009.

36.   Huu Chuc, N.; Thuy, D.V.; Park, J.; Kim, D.; Koo, J.; Lee, Y.; Nam, J.D.; Choi, H.R. In *A dielectric elastomer actuator with self-sensing capability*, Proceedings of SPIE - The International Society for Optical Engineering, 2008.

37.   Rizzello, G.; Naso, D.; York, A.; Seelecke, S. A self-sensing approach for dielectric elastomer actuators based on online estimation algorithms. *IEEE/ASME Transactions on Mechatronics* **2017**, *22*, 728-738.

38.   Hoffstadt, T.; Griese, M.; Maas, J. Online identification algorithms for integrated dielectric electroactive polymer sensors and self-sensing concepts. *Smart Materials and Structures* **2014**, *23*.

39.   Gisby, T. Smart artificial muscles. Doctoral dissertation, The University of Auckland, 2011.

40.   Gisby, T.A.; Calius, E.P.; Xie, S.; Anderson, I.A. In *An adaptive control method for dielectric elastomer devices*, Proceedings of SPIE - The International Society for Optical Engineering, 2008.

41.   Matysek, M.; Haus, H.; Moessinger, H.; Brokken, D.; Lotz, P.; Schlaak, H.F. In *Combined driving and sensing circuitry for dielectric elastomer actuators in mobile applications*, Proceedings of SPIE - The International Society for Optical Engineering, 2011.

42.   Toth, L.A.; Goldenberg, A.A. In *Control system design for a dielectric elastomer actuator: The sensory subsystem*, Proceedings of SPIE - The International Society for Optical Engineering, 2002; pp 323-334.

43. Kujawski, M.; Pearse, J.D.; Smela, E. Elastomers filled with exfoliated graphite as compliant electrodes. *Carbon* **2010**, *48*, 2409-2417.

44. Rosset, S.; Shea, H.R. Flexible and stretchable electrodes for dielectric elastomer actuators. *Applied Physics A: Materials Science and Processing* **2013**, *110*, 281-307.

45. Chiang Foo, C.; Cai, S.; Jin Adrian Koh, S.; Bauer, S.; Suo, Z. Model of dissipative dielectric elastomers. *Journal of Applied Physics* **2012**, *111*.

46. Rosset, S.; O'Brien, B.M.; Gisby, T.; Xu, D.; Shea, H.R.; Anderson, I.A. Self-sensing dielectric elastomer actuators in closed-loop operation. *Smart Materials and Structures* **2013**, *22*.

47. Carpi, F.; Anderson, I.; Bauer, S.; Frediani, G.; Gallone, G.; Gei, M.; Graaf, C.; Jean-Mistral, C.; Kaal, W.; Kofod, G., *et al.* Standards for dielectric elastomer transducers. *Smart Materials and Structures* **2015**, *24*.

48. Li, C.; Xie, Y.; Li, G.; Yang, X.; Jin, Y.; Li, T. Electromechanical behavior of fiber-reinforced dielectric elastomer membrane. *International Journal of Smart and Nano Materials* **2015**.

49. Lu, T.; Huang, J.; Jordi, C.; Kovacs, G.; Huang, R.; Clarke, D.R.; Suo, Z. Dielectric elastomer actuators under equal-biaxial forces, uniaxial forces, and uniaxial constraint of stiff fibers. *Soft Matter* **2012**, *8*, 6167-6173.